Physica 12D (1984) 279–294
North-Holland, Amsterdam

SURFACE UNDULATIONS IN EXPLOSIVE CRYSTALLIZATION: A NONLINEAR ANALYSIS OF A THERMAL INSTABILITY

Wim VAN SAARLOOS and John D. WEEKS
AT&T Bell Laboratories, Murray Hill, New Jersey 07974, USA

We argue that surface undulations observed after self-sustained rapid crystallization of amorphous films result from a thermal instability that induces a periodically varying crystallization rate. Its physical origin is discussed for a simple nonlinear heat conduction model which yields good agreement with experimental observations. The model displays a rich variety of interesting physical phenomena. It contains a co-dimension two bifurcation point in whose vicinity detailed analytic results can be obtained. A numerical analysis of the nonlinear oscillations shows that these, in turn, bifurcate via a series of period-doubling bifurcations.

1. Introduction

Recently, there has been much interest in instabilities occurring during crystal growth, particularly those leading to dendritic growth and the morphological instabilities of the crystal–melt interface [1]. In this paper† we analyze a much simpler thermal instability which can explain phenomena observed during the rapid crystallization of metastable amorphous films. Instead of being a morphological instability along the amorphous to crystalline (a–c) interface of the type discussed at this conference by Sekerka [2], this is a thermal instability in the direction of propagation of the a–c front, and occurs even for straight fronts. As a result, its wavelength is given in terms of a thermal length only.

Under favorable experimental conditions, layers of amorphous Sb [3–8], Ge [9–24], Si [24–28] and other materials [29, 30] can crystallize very rapidly when crystallization is initiated by a laser pulse or by impact with a stylus. The name explosive crystallization stems from the fact that the speed of the crystallization front can be of the order of meters per second. Since crystallization rates are strongly dependent on temperature, it was realized long ago [4] that this phenomenon is associated with the temperature rise induced by the latent heat liberated in the a–c transition. Whether a self-sustained crystallization wave can occur in a particular case therefore depends on an energy balance. If the latent heat liberated is too small or the heat loss to the substrate too great, the crystallization wave cannot sustain itself and dies out. One then has to initiate the process repeatedly by scanning the layer with a laser beam [15–20, 26–28] so that the crystallization front proceeds in bursts: the front first outruns the laser beam, then slows down and stops, after which the process repeats itself when the heat from the moving laser beam catches up [31].

In materials like Sb [3–8], Bi [30] or Yb [30], on the other hand, *self-sustained* crystallization waves have been observed that propagate through the whole layer (often a few micron thick) after being initiated at a single spot. In several of the latter experiments the crystalline phase exhibits periodic variations in the height of the layer [4, 8]. Far from the initiation point, the structure is often essentially one-dimensional, resembling a frozen-in pattern of parallel water waves near a beach. Wickersham *et al.* [8] noted that the undulations could have a thermal origin, since the wavelength λ in their experiments was roughly equal to the thermal length κ/V_{av} (here κ is the thermal diffusivity which we assume for simplicity is the same

†A brief account of this work was given in Phys. Rev. Lett. 51 (1983) 1046.

in the a and c phases, and V_{av} the average crystallization speed). In this paper, we argue that they indeed result from a thermal instability of a steadily advancing a–c front to one with an oscillating growth rate.

In the next section a simple model for explosive crystallization, already studied by Gilmer and Leamy [32], is introduced. The steady state solutions, corresponding to a–c fronts propagating with constant speed, are discussed. In section 3 we analyze the stability of the steady state solutions in qualitative terms, deferring the explicit linear stability analysis to an appendix. It is shown that under certain conditions an oscillatory (Hopf) bifurcation can occur, which leads to solutions with a periodically varying growth rate. The physical mechanism leading to this behavior is discussed. A detailed analytic treatment of the nonlinear behavior of our model is possible in the neighborhood of a particular point (a co-dimension two bifurcation point) where time dependences are slow. This is carried out in section 4. In section 5 we compare our predictions with the experimental observations, and comment on the validity of the model. Section 6 contains a more detailed discussion of successive period doubling bifurcations that were found in a numerical analysis of the nonlinear oscillating solutions.

2. Steady state propagation

In view of the experimental observations that the surface undulations far from the initiation point are often parallel, we analyze the propagation of a straight front, neglecting temperature differences in the vertical and lateral direction and any possible coupling to density and height differences. (We will come back to this in section 4.) In the laboratory frame, the propagation is taken to be in the positive x' direction; it is more convenient, however, to use the coordinate frame $x = x' - \int^t \mathrm{d}t' V(t')$ co-moving with the front so that the a phase is at $x > 0$ and the c phase at $x < 0$. Here V is the interface velocity or growth rate. Using this frame, we follow Gilmer and Leamy [32] and assume a balance equation of the form

$$\frac{\partial T}{\partial t} = \kappa \frac{\partial^2 T}{\partial x^2} + V \frac{\partial T}{\partial x} - \Gamma(T - T^0) + qV\delta(x). \quad (1)$$

Eq. (1) expresses the change in the temperature T in terms of four contributions: The first term on the right-hand side gives the heat conduction through the layer; the second term results from the transformation to the moving frame; the third one crudely describes the heat loss to the substrate at temperature T^0, and replaces the contribution from radiation and heat conduction to the substrate which should be taken into account in a more realistic treatment. The fourth contribution is the source term due to the latent heat LV liberated per unit of time and area at the a–c boundary (here L is the latent heat per unit volume [33]; if C is the specific heat per unit volume, $q = L/C$). The delta function ensures that the latent heat is released only at the a–c boundary at $x = 0$, and is equivalent to the boundary condition $\kappa\, \partial T/\partial x|_{0-} - \kappa\, \partial T/\partial x|_{0+} = qV$. Eq. (1) is supplemented with the boundary condition $T(x, t) \to T^0$ for $x \to \pm\infty$.

Eq. (1) is incomplete until the growth rate V is specified. As usual, we assume that V is an explicit function only of the boundary temperature [34] $T^{\mathrm{b}}(t) \equiv T(x = 0, t)$,

$$V = V(T^{\mathrm{b}}(t)). \quad (2)$$

This "constitutive relation" introduces a nonlinear dependence on T in eq. (1) which causes the instability we discuss below. The appearance of a term $V\,\partial T/\partial x$ with V independent of the position x is typical of moving boundary problems.

For concreteness, we consider a dependence of V on T^{b} as sketched in fig. 1. This is the type of growth rate observed for crystal growth from a melt [34]. The a–c growth rate is thought to be of a similar form, although accurate measurements are only available on the low temperature side where V increases with T^{b} as $V \propto \exp(-Q/T^{\mathrm{b}})$. It is precisely on this side where the thermal instability discussed below occurs.

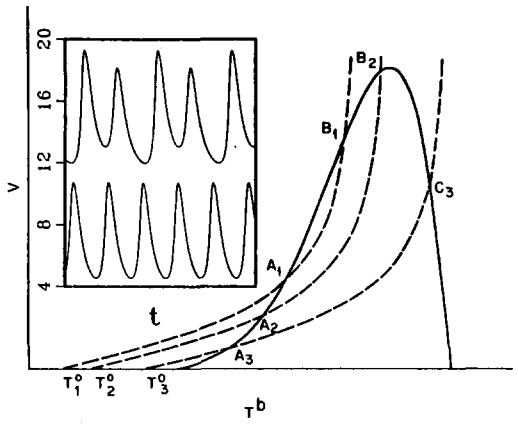

Fig. 1. Solid line: a typical curve for the a–c growth velocity as a function of the a–c boundary temperature. The dashed lines give the relationship between V_{ss} and T_{ss}^b for which eq. (1) has steady state solutions. Inset: V as a function of time for two different values of T^0 which produce oscillatory growth rates. The upper curve (obtained by adding 8 units to V) is a "period 2" solution.

In the steady state, when the a–c boundary is propagating with a constant velocity V_{ss}, it is most convenient first to solve eq. (1) without recourse to eq. (2). In this case, eq. (1) is linear and is solved by an exponential profile of the form $T = T_{ss}^b \exp(-ax)$ for $x > 0$ and similarly for $x < 0$, provided that V_{ss} and T_{ss}^b are related by [32]

$$V_{ss} = 2(\kappa\Gamma)^{1/2}\left(\left(q/\Delta T_{ss}^b\right)^2 - 1\right)^{-1/2}. \tag{3}$$

Here $\Delta T_{ss}^b \equiv T_{ss}^b - T^0$ is the temperature rise at boundary. This function is drawn in fig. 1 with a dashed line for several values of T^0, keeping κ and Γ fixed. For very large steady state velocities, ΔT_{ss}^b approaches the value $q = L/C$, since the heat loss to the substrate is much smaller than the latent heat liberated per unit of time; energy conservation then dictates that $C\Delta T_{ss}^b \simeq L$.

Not all hypothetical V_{ss} satisfying eq. (3) are consistent with the physically possible growth rates given in eq. (2). Thus the actual steady state velocity and boundary temperature are determined by the intersection of these curves, as shown in fig. 1, though the *stability* of these solutions must be investigated. As in the experiments [8], different steady state values are obtained by changing T^0. (In principle, one could alternatively change the value of $\kappa\Gamma$.) If T^0 is too low, the two curves do not intersect, and self-sustained explosive crystallization is not possible.

If one considers V as a given function of time, eq. (1) is a linear partial differential equation for T, whose Green's function can be derived in the standard way [35]. Using this result, the formal solution to eq. (1) can then be written as

$$\begin{aligned}\Delta T^b(t) = q\int_{-\infty}^{0} \mathrm{d}x\,(4\pi\kappa\tau)^{-1/2} \\ \times \exp\left[-\Gamma\tau - x^2/(4\kappa\tau)\right] \\ + \int_{-\infty}^{+\infty} \mathrm{d}x\,(4\pi\kappa t)^{-1/2} \exp\left\{-\Gamma t \right. \\ \left. - \left(x - \int_0^t V(t')\,\mathrm{d}t'\right)^2 \Big/ 4\kappa t\right\} \Delta T(x,0),\end{aligned} \tag{4}$$

where $\tau \equiv \tau(x,t)$ is implicitly given by

$$x = -\int_{t-\tau}^{t} \mathrm{d}t' V(T^b(t')). \tag{5}$$

Eqs. (4) and (5) have the following interpretation in the lab frame. The heat released at previous positions of the moving a–c boundary spreads out due to conduction and heat loss as a damped Gaussian, and so can still contribute to the present boundary temperature. Eq. (5) determines the time τ elapsed since the boundary passed a position a distance $|x|$ to the left of the present position of the boundary, and the first term in the right-hand side of eq. (4) gives the sum of all the contributions to T^b from the heat previously released. The second term in the right-hand side of eq. (4) results from the initial conditions at $t = 0$. This interpretation of eqs. (4) and (5) will be helpful in the discussion of the linear stability analysis below.

3. Stability analysis of the steady state solutions

We now investigate the stability of the possible steady state solutions obtained above. We argue

qualitatively that an oscillatory (Hopf) bifurcation of one of the steady state solutions can occur, and discuss the physical origin of the resulting oscillatory solutions. The detailed linear stability analysis supporting the qualitative discussion of this section is given in appendix A.

In the following, we will distinguish between the three different types of intersections, labeled A, B and C in fig. 1. Consider C first. As already argued by Gilmer and Leamy [32] the steady state solutions at this point should be *stable*, since a small increase in T^b results in a smaller velocity from eq. (2), and the resulting decrease in liberation of latent heat will bring the boundary temperature back to its steady state value at C. Using the same argument, we expect the points A to be *unstable*.

However, the most interesting behavior occurs for points B, where changes in the heat flow and heat loss as well as the heat generated by a perturbation must be taken into account in a stability analysis. Consider the steady state at B_2 where the slope of the growth rate curve is small but positive. Here a large increase in T^b, and so a relatively large increase in heat loss and heat flow away from the boundary, is associated with only a small increase in velocity (and so heat generation). We therefore expect this point to be *stable*. For intersections with a large slope, like B_1, the situation is reversed and these points should therefore be *unstable*, provided that Γ is not too large.

These elementary considerations are supported by the explicit linear stability analysis of appendix A, the main results of which are summarized in fig. 2. In this stability diagram, $(\Delta T_{ss}^b/V_{ss})(dV/dT^b) \equiv \alpha$, the (dimensionless) slope of the growth rate curve in the steady state point, is plotted along the horizontal axis and $(\Delta T_{ss}^b/q)^2 = (4\kappa\Gamma/V_{ss}^2 + 1)^{-1} \equiv \beta$ along the vertical axis. Here β is a measure of the ratio of the thermal diffusion time $4\kappa/V_{ss}^2$ and the relaxation time Γ^{-1} and varies between 0 and 1. In agreement with the physical arguments given above, steady state points C are stable, and those of type A unstable. The ones of type B become unstable in the case $\beta > 2/3$ (or $\Gamma < V_{ss}^2/8\kappa$) when

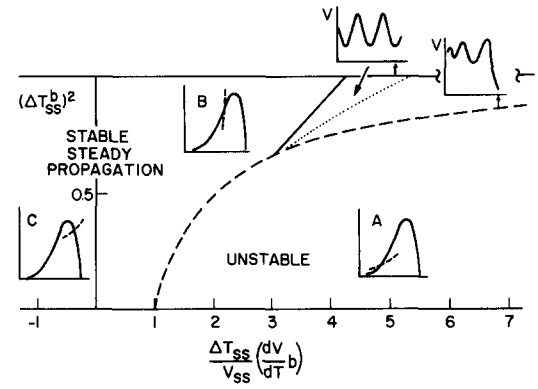

Fig. 2. Stability diagram for the various steady state solutions whose locations on the growth rate curve are schematically indicated. The (dimensionless) slope of the function (2) in the steady state point is plotted along the horizontal axis and $(\Delta T_{ss}^b)^2$ (in units of q^2) along the vertical axis. The dashed line separates the points denoted by A and B in fig. 1. The steady state points B to the right of the solid line are unstable. However, in this region the full nonlinear equations can admit either stable oscillatory solutions (to the left of the dotted line) or solutions that die out (for points B to the right of the dotted line). The behavior of the velocity in both cases is schematically indicated.

the dimensionless slope (plotted along the horizontal axis) reaches some value between 3 and $2 + \sqrt{5} \approx 4.236$. The instability occurring when the point B moves to the right of the solid line is of oscillatory (Hopf) type: for values of the slope larger than the critical value, the boundary temperature and speed of the front oscillate periodically in time (see the inset of fig. 1). (These solutions will be discussed in more detail later.)

It is easy to understand why the instability at steady state points B on the solid line is of Hopf type so that the linearized equations have a purely imaginary eigenvalue. At points B, the slope of the growth rate curve dV/dT^b is, by definition, smaller than the slope of the curve of steady state points: $dV/dT^b < dV_{ss}/dT_{ss}^b$†. Suppose on the contrary that the eigenvalue of the equations, linearized around the steady state solutions B, could be real. Then there would exist solutions of the form $T^b \approx$

†Points of type A are defined by $dV/dT^b > dV_{ss}/dT_{ss}^b$, and the dashed line in fig. 2 is given by the equation $dV/dT^b = dV_{ss}/dT_{ss}^b$.

$T_{ss}^b + \epsilon \exp(\omega t)$ and $V \simeq V_{ss} + (dV/dT^b)\epsilon \exp(\omega t)$ with ω real and, close to the solid line, arbitrarily small. In the limit $\omega \to 0$, however, the perturbed temperature field must obey the same equation as the steady state solutions, and hence one would also have up to linear order in ϵ, $V \approx V_{ss} + (dV_{ss}/dT_{ss}^b)\epsilon \exp(\omega t)$ for ω small. Since at points B, $dV/dT^b < dV_{ss}/dT_{ss}^b$, this is obviously impossible. We therefore conclude that near the solid line in the diagram, ω must be complex.

The above analysis implies the following picture. At high enough substrate temperatures, T_3^0 in fig. 1 say, the intersection at A is unstable and the one at C stable. Hence, after initiation of the process, the a–c front will propagate with a speed determined by the intersection C. If T^0 is lowered to T_2^0, say, the intersection B_2 is still stable since the slope of the growth rate curve is relatively small, and the front continues to advance with constant speed. However, if T^0 is lowered to T_1^0, say, the slope of the growth rate curves is large enough that steady state propagation is no longer possible. In this case we find that self-sustained explosive crystallization fronts propagate with a periodically varying growth rate.

In a numerical analysis of these nonlinear oscillatory solutions, we have found that two things can happen in cases where T^0 is lowered even more so that the slope becomes even larger. One effect arises from the fact that the amplitude of the oscillations grows larger and larger as T^0 is lowered. Indeed, it finally becomes so large that the front stops propagating because T^b drops too much at the minima. This is schematically indicated in fig. 2 by the dotted line. Solutions to the right of this line eventually die out. Thus, self-sustained explosive crystallization does not occur in every case where the two curves in fig. 1 intersect. This nonlinear effect is analyzed in the next section in the neighborhood of the bifurcation point where the three lines of fig. 2 intersect. There we will determine the slope of the dotted line near this point. Away from this point, the conditions under which the oscillations die out depend on the detailed shape of the growth rate curve. Secondly, it turns out that the periodic solutions undergo period doubling bifurcations in the region of fig. 2 between the solid and dotted line. These bifurcations will be discussed in section 6.

Having understood the stability, it remains to understand the physical origin of the oscillations and to get an estimate for their period. In the steady state, when eq. (5) reduces to $|x| = V_{ss}\tau$, the main contribution in the first integral in (4) comes from those positions x for which $\Gamma\tau + x^2/4\kappa\tau \lesssim 2$, or

$$\tau \lesssim \frac{2}{\Gamma + V_{ss}^2/4\kappa} \equiv \tau_m. \tag{6}$$

Contributions to T^b from positions further back than $d_m \equiv V_{ss}\tau_m$ are essentially negligible. In the regime $\Gamma \ll V_{ss}^2/4\kappa$, τ_m sets the timescale over which changes in T^b take place. Hence we expect the period of the oscillations to be of the order of $\tau_m \approx 8\kappa/V_{ss}^2$. Note that the "memory time" τ_m becomes shorter the larger the velocity is, since the boundary moves more rapidly out of the region that can be reached by heat conduction. To understand the oscillatory solutions, consider a small perturbation with an increased velocity around a steady solution in the case of small damping ($\Gamma \ll V_{ss}^2/4\kappa$). A small decrease in τ makes a Gaussian $\tau^{-1/2}\exp(-y^2/4\tau)$ narrower: the center increases whereas the wings at $|y| > (2\tau)^{1/2}$ decrease. For the (slightly damped) Gaussians in the integrand of eq. (4) with $|x| < 2\kappa/V_{ss} = d_m/4$ the perturbation therefore results in an increase of T^b, while it decreases the contributions of those at distances further away†. Thus, when the growth rate speeds up, the boundary can move ahead so rapidly that the heat diffusion from positions not immediately behind the boundary can not keep up. Consequently, T^b and the front velocity drop, after which more heat diffuses towards the boundary, and the velocity can rise again.

†In the opposite case ($\Gamma > V_{ss}^2/4\kappa$) all damped Gaussians in eq. (4) respond similarly to a perturbation and all disturbances decay monotonically.

4. Behavior close to the bifurcation point $\alpha = 3$, $\beta = 2/3$

In the last section, we found two lines in the linear stability diagram where the stability changes. Along the solid line drawn in fig. 2 where $\beta = (\alpha - \alpha^{-1})/4$, we found a Hopf bifurcation. Hence, for perturbations in T^b of the form $T^b = T^b_{ss} + \varepsilon e^{2\omega t/\tau_m}$, the two eigenvalues $\omega_\pm$ along the solid line satisfy $\mathrm{Re}\,\omega_\pm = 0$, $\mathrm{Im}\,\omega_\pm \neq 0$. Moreover, one eigenvalue always vanishes along the dashed line, where $\beta = 1 - \alpha^{-1}$ and the A and B points coincide. The two lines intersect at $\alpha = 3$, $\beta = 2/3$. As a result, both eigenvalues vanish at this point, which means that it is a co-dimension two bifurcation point [36–40]. Using the fact that the time-dependences are slow, we can carry out a detailed analytic investigation of the behavior of the system in the neighborhood of such a point. Note that the growth rate curve (2) and the curve of steady state points (3) have equal slopes at points on the dashed line in fig. 2. Thus we analyze how the change of stability at B takes place in the special case in which the curves (2) and (3) are nearly tangent, so that the intersections A and B lie close together. Readers primarily interested in physical implications of our analysis can skip to section 4.3.

4.1. *Reduction to the normal form of a co-dimension two bifurcation*

For small $\delta\alpha \equiv \alpha - 3$ and $\delta\beta \equiv \beta - 2/3$ we explicitly find from the result for $\omega_\pm$, given in eq. (A.7)

$$\frac{2}{\tau_m}\omega_\pm \approx -(18\delta\beta - 5\delta\alpha) \pm \sqrt{24(\delta\alpha - 9\delta\beta)}\,. \quad (7)$$

The two slow modes associated with these small eigenvalues give the dominant behavior for long times. The time dependence of the system in the neighborhood of the bifurcation point is therefore described by a second order equation of the form

$$\ddot{v} - \lambda_2\dot{v} - \lambda_1 v = F(v, \dot{v}), \quad (8)$$

with λ_1 and λ_2 small and F vanishing at the bifurcation point. Here $v \equiv V/V_{ss} - 1$ is the deviation from the steady state velocity and the nonlinear function F is yet to be determined. From the requirement that the eigenvalues of the $\dot{v} = v = 0$ fixed point in (8) coincide with (7), we get up to lowest order the identification

$$\lambda_1 = 24(\delta\alpha - 9\delta\beta), \quad \lambda_2 = -2(18\delta\beta - 5\delta\alpha). \quad (9)$$

In the absence of symmetries, the function F will be of the form $F = a_1 v^2 + a_2 v\dot{v} + a_3\dot{v}^2$, keeping only terms of second order in smallness. The coefficients a_1, a_2 and a_3 are determined in appendix B by expanding the integral solution about the bifurcation point. We find

$$a_1 = -72\left(1 - \frac{1}{18}V''\right), \quad a_2 = 144, \quad a_3 = -75/2, \quad (10)$$

where

$$V'' \equiv \frac{(\Delta T^b_{ss})^2}{V_{ss}} \frac{d^2V}{(dT^b)^2} \quad (11)$$

is the (dimensionless) second derivative of the growth rate curve in the steady state.

By performing a transformation to the variable $y = v + \frac{1}{2}a_3 v^2$ in eq. (8), we can eliminate the term proportional to $\dot{v}^2$, while to second order all the other terms are unchanged. Introducing the variables $y_1 = y$, $y_2 = \dot{y}$, eq. (8) can thus be rewritten as the set of first order equations

$$\dot{y}_1 = y_2, \quad (12)$$

$$\dot{y}_2 = \lambda_1 y_1 + \lambda_2 y_2 + a_1 y_1^2 + a_2 y_1 y_2, \quad (13)$$

and it is convenient to study the trajectories in the y_1, y_2 plane. The above set of equations is the normal form of one of the two possible co-dimension two bifurcations with quadratic nonlinearities [37].

4.2. *Analysis of the normal form*

Eqs. (12) and (13) have two fixed points, $y_1 = 0$, $y_2 = 0$ and $y_1 = -\lambda_1/a_1$, $y_2 = 0$, whose stability is

related by a symmetry: if we perform the transformation $w_1 = y_1 + \lambda_1/a_1$, $y_2 = w_2$, then w_1 and w_2 obey, up to the relevant order, the same equations as y_1 and y_2 but with λ_1 replaced by $-\lambda_1$ and λ_2 replaced by $\lambda_2 - \lambda_1 a_2/a_1$. Hence the global behavior of eqs. (12) and (13) can be obtained using only the behavior for $\lambda_1 < 0$ by interchanging the role of the fixed points and rescaling λ_2.

We summarize the results of a linear stability analysis of eqs. (12) and (13) and the connection with the stability analysis of section 3 as follows: (i) If $\lambda_1 > 0$, the $y_1 = y_2 = 0$ fixed point is unstable (for $\lambda_1 > 0$, $\delta\alpha > 9\delta\beta$ implies that we are below the dashed line in fig. 2, and the point $y_1 = y_2 = 0$ corresponds to an A point). Because of the symmetry, the $y_1 = -\lambda_1/a_1$, $y_2 = 0$ fixed point is always unstable for $\lambda_1 < 0$. (ii) If $\lambda_1 < 0$ and $\lambda_2 < 0$, the fixed point $y_1 = y_2 = 0$ is stable (a B point left of the solid line). Along the line $\lambda_1 < 0$, $\lambda_2 = 0$ there is a Hopf bifurcation, and for $\lambda_1 < 0$, $\lambda_2 > 0$, the fixed point is unstable (a B point right of the solid line).

The limit cycle that bifurcates from the $y_1 = y_2 = 0$ fixed point along the line $\lambda_2 = 0$, $\lambda_1 < 0$ does not exist for all values of λ_1 and λ_2 in the second quadrant: if the limit cycle grows so large that it crosses the other unstable fixed point at $y_2 = 0$, $y_1 = -\lambda_1/a_1$, it becomes unstable. Following Guckenheimer [36, 37], we now determine the values of the parameters for which this happens.

We take advantage of the smallness of λ_1 and λ_2 by introducing the scaling

$$\lambda_1 = \mu^2 \Lambda_1, \quad \lambda_2 = \mu^2 \Lambda_2, \quad \mu t = T,$$
$$y_1 = \mu^2 Y_1, \quad y_2 = \mu^3 Y_2, \tag{14}$$

so that eqs. (12) and (13) become

$$\dot{Y}_1 = Y_2, \tag{15}$$
$$\dot{Y}_2 = \Lambda_1 Y_1 + a_1 Y_2^2 + \mu(\Lambda_2 Y_2 + a_2 Y_1 Y_2). \tag{16}$$

We will investigate the limit cycle around the $Y_1 = Y_2 = 0$ fixed point in the left half plane $\Lambda_1 < 0$. For $\mu = 0$ the above equations reduce to the Hamilton equations corresponding to the Hamiltonian

$$H = \tfrac{1}{2} Y_2^2 - \tfrac{1}{2}\Lambda_1 Y_1^2 - \tfrac{1}{3} a_1 Y_1^3. \tag{17}$$

To zeroth order in μ, the integral curves of eqs. (15) and (16) are therefore the lines of constant energy $H(Y_1, Y_2) = \text{constant}$.

Since areas are conserved by a Hamiltonian flow, the contraction or expansion of an area A under the flow given by eqs. (15) and (16), depends only on the terms proportional to μ,

$$\frac{dA}{dt} = \mu \int_A dY_1 dY_2 \, (\Lambda_2 + a_2 Y_1). \tag{18}$$

Obviously, the area enclosed by a limit cycle does not change in time,

$$\mu \int_{\text{l.c.}} dY_1 dY_2 \, (\Lambda_2 + a_2 Y_1) = 0. \tag{19}$$

When evaluating this expression to lowest order in μ, the limit cycle may be approximated by its $\mu = 0$ limit, i.e. by the integral curve of the Hamiltonian system. Thus, for a given set of parameters, eq. (19) enables us to select the limit cycle from the set of curves $H(Y_1, Y_2) = \text{constant}$ [41].

As stated before, the limit cycle disappears if it intersects the second unstable fixed point at $Y_1 = -\Lambda_1/a_1$ (its period then goes to infinity). To determine the set of parameters for which this happens up to lowest order in μ, we therefore have to evaluate eq. (19) in the approximation that the limit cycle is the integral curve $H(Y_1, Y_2) = H(-\Lambda_1/a_1, 0)$, or

$$Y_2 = \pm \left[\frac{2a_1}{3} \left(Y_1 + \frac{\Lambda_1}{a_1} \right)^2 \left(Y_1 - \frac{\Lambda_1}{2a_1} \right) \right]^{1/2} \qquad (\Lambda_1 < 0). \tag{20}$$

Using this result in eq. (19) we find that the limit cycle in the left half plane $\Lambda_1 < 0$ disappears for

parameter values such that

$$\int_{-\Lambda_1/a_1}^{\Lambda_1/2a_1} dY_1\, 2\left[\frac{2a_1}{3}\left(Y_1+\frac{\Lambda_1}{a_1}\right)^2\left(Y_1-\frac{\Lambda_1}{2a_1}\right)\right]^{1/2} \times(\Lambda_2+a_2Y_1)=0, \quad (\Lambda_1<0), \tag{21}$$

or, after an elementary integration,

$$\frac{\Lambda_2}{\Lambda_1}=\frac{1}{7}\frac{a_2}{a_1} \quad (\Lambda_1<0). \tag{22}$$

If a_2/a_1 is negative, this result shows that the limit cycle disappears along a straight line in the second quadrant of the λ_1, λ_2 plane, indicated by L_3 in fig. 3. Taking also into account the behavior in the right half plane ($\lambda_1 > 0$) which follows from the symmetry of the equations discussed after eq. (13), we now arrive at the following global picture in the neighborhood of the bifurcation point in the case $a_1/a_2 < 0$. In region IV of fig. 3, the system exhibits one stable and one unstable fixed point.

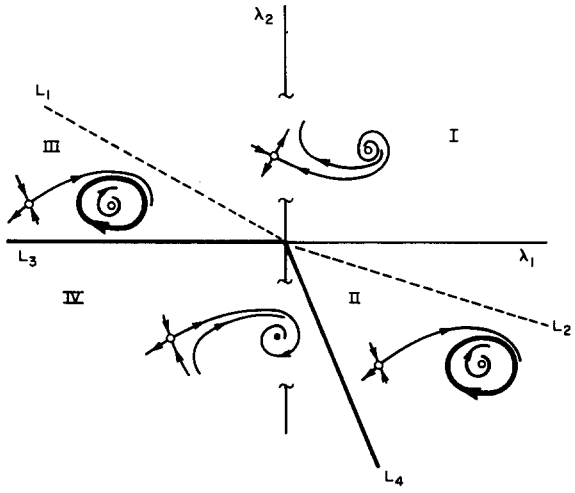

Fig. 3. Schematic phase portrait of the behavior of the normal form of the codimension two bifurcation with quadratic nonlinear terms, showing the different characteristic behavior for various values of λ_1 and λ_2 in the case $a_1/a_2 < 0$. Following ref. 39, the typical phase space orbits and the attractors in the y_1, y_2 plane are drawn with the convention that solid circles denote stable fixed points, open ones unstable fixed points, and a thick solid line a stable limit cycle. Orbits are drawn as thin solid lines. In the case $a_1/a_2 > 0$ there are no stable limit cycles.

The stable fixed point bifurcates along the line L_3 ($\lambda_2 = 0$, $\lambda_1 < 0$) to a stable limit cycle as depicted in region III, and along the line L_4 ($\lambda_2/\lambda_1 = a_2/a_1$) to the limit cycle of region II. When λ_2 becomes larger for fixed λ_1, the size of the limit cycle grows until it finally encounters the second unstable fixed point. This happens along the lines L_1 ($\lambda_2/\lambda_1 = a_2/7a_1$) and L_2 ($\lambda_2/\lambda_1 = 6a_2/7a_1$). For even larger values of λ_2 we are in region I, and since there are then no stable fixed points and limit cycles, higher order terms have to be taken into account for a complete description of the system.

Eqs. (12) and (13) are also invariant under a change of sign in y_2, λ_2, a_2 and t. Hence, the behavior of the system for $a_1/a_2 > 0$ can be obtained from the one for $a_1/a_2 < 0$ by inverting the stability of all fixed points and limit cycles because of the change in sign of the time t. In particular, there are no stable limit cycles in the case $a_1/a_2 > 0$.

4.3. *Implications for our model*

In our model, we have from eq. (10) $a_1/a_2 = -\frac{1}{2}(1 - V''/18)$. In cases of practical interest, V'' is small and this ratio is negative. (If $V'' > 18$ the curvature of the growth rate curve is so large that (2) and (3) have three rather than two intersections.) Then the global behavior near the bifurcation point is as depicted in fig. 3, and comparison with fig. 2 shows the following. According to eq. (9), the line $\lambda_2 = 0$, $\lambda_1 < 0$ where the Hopf bifurcation occurs coincides with the slope of the solid line ($d\beta/d\alpha = 5/18$) near the point $\alpha = 3$, $\beta = 2/3$ in fig. 2. In fig. 3, the stable limit cycle in region III disappears along the dotted line L_1, and consequently in fig. 2 along a line with slope $d\beta/d\alpha = 59/342$ for $V'' = 0$, and the region to the right of the dotted line in fig. 2 is related to region I of fig. 3. Since there are in general only two steady state solutions in our model, the absence of a limit cycle and stable fixed points in region I is in agreement with the numerical observation described in sec-

tion 3 that the a–c front can cease propagating even though the two curves in fig. 1 intersect.

We emphasize that figs. 2 and 3 display different results. Fig. 3 is only valid in the neighborhood of the bifurcation point and shows the *global* nonlinear behavior of the solutions, which depends on the interplay of the two nearby fixed points. Fig. 2, on the other hand, gives the *linear* stability of *each* steady state point regardless of the stability and location of the other intersection. As a result, the analogues of the lines L_2 and L_4 are absent in the region below the dashed curve in fig. 2, since they describe the behavior of a nearby point of type B, not of the one of type A.

5. Comparison with experimental observations

Since there are considerable density differences between the a and c phase, it is likely that the predicted oscillations in T^b and V are the cause of the surface undulations and compositional variations, through differences in grain size or the extent of completeness of the a–c transformation [42]. Note that the slope of the growth rate is large when the oscillatory instability occurs. As a result there are large variations in the growth rate (of order 10 to 50 percent) which would be expected to affect the morphology of the growing crystal. Assuming this to be the case we can compare our results with the following experimental observations of Wickersham et al. [8].

i) In agreement with the arguments given in section 3, the linear stability analysis shows that the period of the oscillations is of the order τ_m. Consequently, we get for the wavelength λ of the oscillations in the regime where $\Gamma \ll V_{ss}^2/4\kappa$ [see eq. (A.9)] $\lambda \approx 6\kappa/V_{av}$. Here we have replaced V_{ss} by the average velocity. This estimate is in reasonable agreement with the experimental values measured [8].

ii) Let T^* be the substrate temperature above which self-sustained explosive crystallization is possible. For T^0 slightly above T^*, say $T^0 = T_1^0$, as shown in fig. 1, the slope at B_1 is steep and the growth rate will oscillate. If T^0 increases to T_2^0, say, the point B_2 becomes stable. Thus, in our model, the oscillations occur for T^0 slightly above T^* and cease at higher temperatures, much like the experimental observation that the "surface roughness was found to decrease as the triggering temperature was increased above T^*" [8].

In principle, our predictions may be tested experimentally by monitoring the growth rate using the differences in optical properties in the a and c phase [20].

As discussed in section 3 the oscillatory behavior can only occur in the regime $\Gamma < V_{ss}^2/8\kappa$, where the thermal diffusion time κ/V_{ss}^2 is much shorter than the relaxation time Γ^{-1} associated with heat losses. This means that for the effect to be seen in an experiment, the heat loss to the substrate within a time of the order of the thermal diffusion time ought to be relatively small. Layers that are too thin can not satisfy this condition. In the case that radiation is negligible, one can make a rough (conservative) estimate of how thick a layer should be. Let us assume that the substrate is a good heat conductor so that it remains always at temperature T^0. After the a–c boundary has passed, the temperature on the bottom part of the layer will decrease as a result of the heat conduction to the substrate. The thickness of the region affected after at time τ_m is of the order of $\sqrt{\kappa\tau_m}$, and the effect of heat loss is small if this length is smaller than the thickness d of the layer. Since $\kappa\tau_m \approx 8\kappa^2/V_{ss}^2 \approx \lambda^2/8$, the instability should thus occur in layers for which $d \gtrsim \lambda$.

In explosive crystallization in Ge, the a phase probably melts first before crystallizing [32, 22, 15]. Whether the same happens in Sb is not clear, but experiments on Yb and Bi [30] at liquid He temperatures seem to rule out the presence of a liquid zone in these materials. In our analysis, we have not taken the possible existence of such a liquid zone into account. However, since these liquid regions are probably much smaller than the wavelength of the undulations [32, 22, 15], we believe their presence would not modify the thermal instability qualitatively.

Up to now, we have based the analysis on the assumption that the a–c boundary remains straight. To investigate qualitatively the possibility of having a Mullins–Sekerka [43, 1, 2] type instability along the front, consider a stable steady state on the left hand side of the growth rate curve (e.g. point B_2 in fig. 1). The temperature profile in front of the a–c boundary drops off rapidly, roughly as $T_{ss}^{b}\exp(-V_{ss}x/\kappa)$. Hence, if there is a small perturbation along the front, the boundary at points bulging forward will be at a lower temperature and will therefore grow less rapidly (we neglect the effect of curvature on the growth rate). This will act to counter the perturbation. In steady state points of type C, however, the situation is different: here the growth will be more rapid at a spot bulging forward. The straight front will now be unstable and break up into protrusions with a typical length determined by a capillary length and the thermal length κ/V_{ss} (the slope of the temperature in front of the boundary). The observation by Leamy et al. [22] that the surface of explosively crystallized Ge layers showed undulations that "are composed of froth-like bubbles that are aligned in irregular rows" [22] may be related to such effects.

In conclusion, when the growth rate increases with increasing temperature we expect the thermal instability discussed before without major changes resulting from a morphological instability along a front. However, on the right-hand side of the growth rate curve, there is no thermal instability, but there will exist significant morphological instabilities that invalidate the use of a simple one-dimensional model.

6. Period-doubling bifurcations

In a numerical study of the nonlinear periodic solutions given by eqs. (1) and (2), we have found that these, in turn, bifurcate via a sequence of period-doubling bifurcations. These Feigenbaum sequences [45] have been analyzed mostly in models with a finite-dimensional phase space. The model studied here for the "infinite-dimensional" temperature field is simple enough to permit a detailed numerical analysis. Here, we discuss an example for one set of parameters obtained by an algorithm described in appendix C. In a future publication we hope to come back to the derivation of an approximate set of ordinary differential equations in a three-dimensional phase space for this system.

In this section, all quantities will be given in dimensionless units: temperatures are measured in units of q, time in units of Γ^{-1}, length in units of $\sqrt{\kappa/\Gamma}$, and hence velocities in units of $\sqrt{\kappa\Gamma}$. The function $V(T^{b})$ used in our specific calculations is

$$V = D\mathrm{e}^{-Q/T^{b}}\left(1-\mathrm{e}^{-L(1/T^{b}-1/T^{M})}\right). \tag{23}$$

Such a functional dependence of V on T^{b} is typical for the growth of a crystal from a melt [34]. In the example discussed here, $T^{M}=1.8$ and $L=3$, and D and Q are adjusted such that the maximum growth velocity of 12 is reached for $T^{b}=1.6$.

In our numerical calculations, we vary the substrate temperature T^{0}. If we decrease T^{0} starting from a relatively large value, the steady state solution becomes unstable at $T^{0}=0.431626$. At this point, $(\Delta T_{ss}^{b})^{2}\approx 0.934$. For lower values of T^{0}, we first observe stable periodic solutions of the type shown in the inset of fig. 1. When lowering T^{0} even more, period-doubling bifurcations are observed. The bifurcation to a period 2 solution occurs at $T^{0}=0.426884$. We have been able to follow the successive bifurcations to period 4, 8 and 16 at $T^{0}=0.4266355$, 0.4266035 and 0.4265965, respectively†. These values seem to converge rapidly to the Feigenbaum ratio δ. At slightly lower temperatures we enter an apparently chaotic regime where no periodicity is evident. (Lowering T^{0} still further finally causes us to cross the dotted line in fig. 2 and the crystallization wave eventually stops.)

†These values of T^{0} depend slightly on the size of the time step used in the calculation, but the qualitative picture is the same for any small step size.

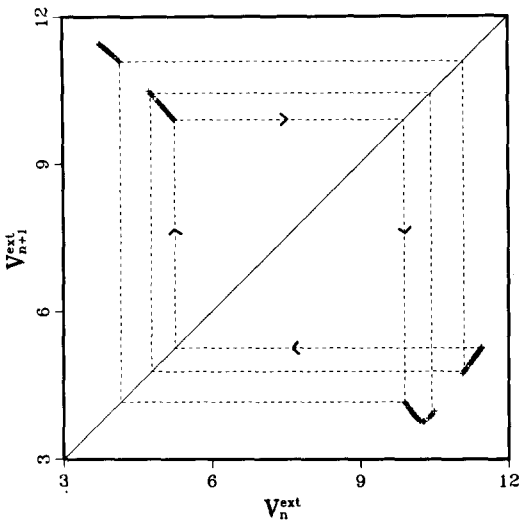

Fig. 4. Plot of V_{n+1}^{ext} as a function of V_n^{ext}. All data points obtained after the initial value term in eq. (4) becomes negligible are included. Here $T^0 = 0.426586$, slightly below the value of T^0 where chaotic behavior sets in. A few iterations of the map are indicated by the dashed lines.

Let V_n^{ext} be the value of the velocity V in the nth extremum (maximum or minimum) of a solution of the equations (1) and (2). Empirically, we found

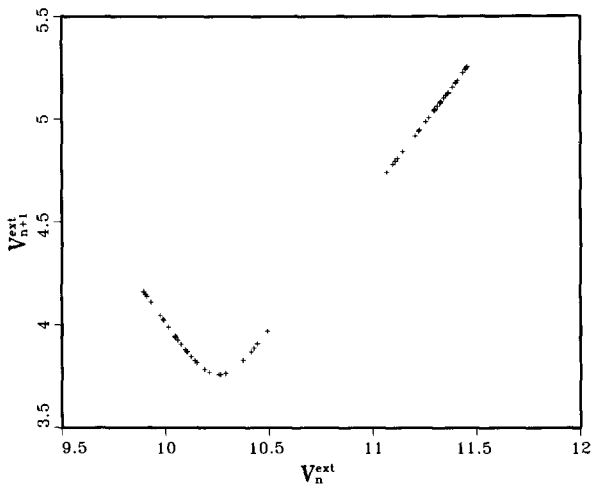

Fig. 5. Enlargement of the lower right hand corner of fig. 4.

that the above observations can be understood within the context of the map obtained by plotting V_{n+1}^{ext} as a function of V_n^{ext}. As shown in figs. 4 and 5, these points turn out to lie on a single curve. Hence in this regime the model is well described by a single valued function f such that

$$V_{n+1}^{ext} = f(V_n^{ext}). \tag{24}$$

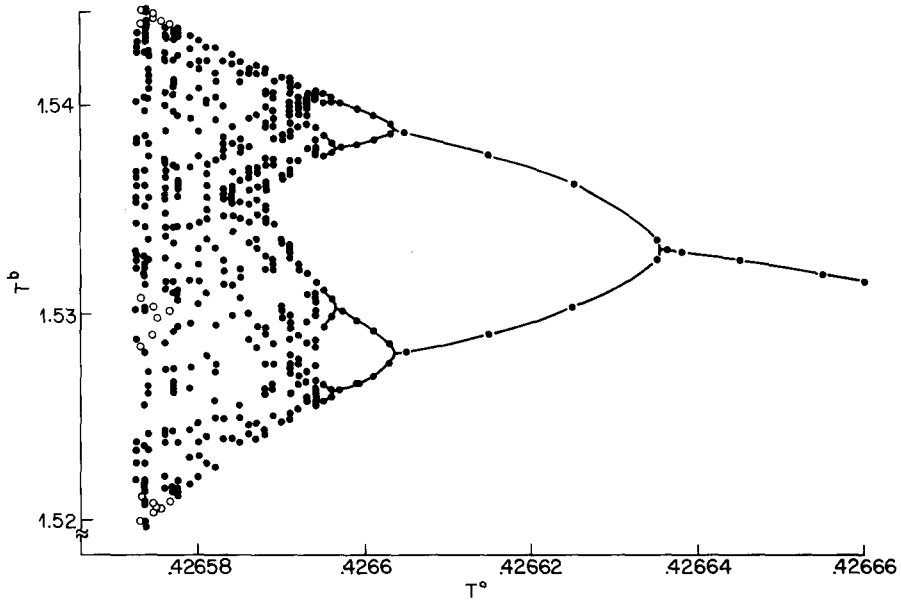

Fig. 6. Values of T^b in the maxima of the oscillations as a function to T^0. Only data points for times larger than about 20 basic periods of the system are included, so that the solutions have relaxed towards the stable periodic solutions, if these exist. Since only points on the upper branch where $11 \lesssim V_n^{ext} \lesssim 11.5$ are shown, the points on the right are actually period 2 solutions. Open circles denote period 6 and 12 solutions. The solid line is merely drawn to guide the eye.

Moreover, this one-dimensional map has indeed a parabolic minimum, characteristic of the Feigenbaum map [45] that explains the occurrence of period doublings. A plot of T^b in the successive maxima of the solutions also shows the characteristic behavior of period doubling bifurcations (fig. 6). Note the following features:

i) There are no indications that a higher dimensional map is needed to describe the system better, because the points defined by the above map appear to lie on a single line to a high degree of accuracy. The fact that the memory time τ_m, defined in eq. (6), is of the same order as the period of the oscillations, is probably the reason this system is described so accurately by a one-dimensional map.

ii) The function f appears to be independent of the initial conditions; moreover, as soon as the initial value term in eq. (4) is negligible, the points of the map lie on the single curve. Thus the system converges very rapidly to the behavior described by (24).

iii) The existence of a minimum in the function f may be related to curvature of the growth rate curve. Even though the maximum velocity is never reached in our numerical solutions (in the calculations described here, the maximum is 12), we did not observe a minimum in f and period doubling bifurcations in calculations when we had modified the function $V(T^b)$ so that it increased linearly with T^b for large boundary temperatures.

Acknowledgements

We are grateful to P.C. Hohenberg, G.H. Gilmer, K.A. Jackson and D.S. Fisher for helpful discussions and to J. Guckenheimer for useful correspondence. We particularly benefitted from a conversation with P.C. Hohenberg on co-dimension two bifurcations.

Appendix A

Linear stability analysis

In this appendix we consider a small perturbation $\Delta T(x,0)$ around the steady state solution $T_{ss}(x)$ at $t=0$, and investigate the behavior of T^b for large t. We assume that $\Delta T(x,0)$ is negligible for x large enough. In that case, the dominant contribution from the initial value term in eq. (4) decays for large t as

$$t^{-1/2}e^{-2t/\tau_m}. \tag{A.1}$$

The asymptotic decay of T^b is therefore at least of this order. Our strategy is to try to find a more slowly decaying mode of the form

$$T^b(t) = T^b_{ss} + \epsilon e^{2\omega t/\tau_m}, \quad V(t) = V_{ss} + \epsilon V' e^{2\omega t/\tau_m}, \tag{A.2}$$

with $\mathrm{Re}\,\omega > -1$. Here $V' \equiv dV/dT^b$ is the derivative of (2) in the steady state point and ϵ is assumed to be small. We have verified that the steady state solutions are indeed stable with perturbations decaying asymptotically as (A.1) if there are no solutions of the form (A.2).

By substituting eq. (A.2) into eq. (5) and linearizing, one finds for the resulting change $\delta\tau(x,t)$ in τ

$$\delta\tau = \frac{-\epsilon V'\tau_m}{2\omega V_{ss}} \exp(2\omega t/\tau_m)(1 - \exp(2\omega x/V_{ss}\tau_m)), \tag{A.3}$$

where we used the fact that $x = -V_{ss}\tau$ in the steady state. Upon linearization of eq. (4), one gets by

neglecting the initial value term

$$\epsilon e^{2\omega t/\tau_m} = \frac{q\epsilon V'}{4\kappa^{1/2}V_{ss}^{1/2}\omega} e^{2\omega t/\tau_m} \times \int_{-\infty}^{0} dx\,(1-\exp(2\omega x/V_{ss}\tau_m))\frac{1}{|x|^{3/2}}\left(\frac{1}{2}V_{ss} - \left(\Gamma - \frac{V_{ss}^2}{4\kappa}\right)x\right)\exp(2x/V_{ss}\tau_m)$$

$$= \frac{qV'\epsilon}{2(2\pi\kappa\tau_m)^{1/2}\omega} e^{2\omega t/\tau_m}\int_0^{\infty} dy\,(1-e^{-y\omega})\left(-\frac{d}{dy}(y^{-1/2}e^{-y}) - \frac{V_{ss}^2}{4\kappa}\tau_m y^{-1/2}e^{-y(1+\omega)}\right). \quad (A.4)$$

After a partial integration, we are left with elementary integrations. Evaluating these, we arrive at the basic relation

$$1 = \alpha\left[-\frac{2\beta}{\omega} + \left(1+\frac{2\beta}{\omega}\right)(1+\omega)^{-1/2}\right]. \quad (A.5)$$

The parameters α and β used here have the same meaning as in section 3; $\alpha \equiv qV'/(8\kappa\tau_m)^{1/2} = V'\Delta T_{ss}^b/V_{ss}$ is the dimensionless slope of the growth rate curve and $\beta \equiv V_{ss}^2\tau_m/4\kappa = (4\kappa\Gamma/V_{ss}^2+1)^{-1} = (\Delta T_{ss}^b/q)^2$. Eq. (A.5) can be written in the "semiquadratic" [44] form

$$(1+\omega)^{1/2} = (\omega+2\beta)/(\omega/\alpha+2\beta). \quad (A.6)$$

After taking the square of this equation, and rearranging, one arrives at a quadratic equation for ω with roots

$$\omega_{\pm} = -\tfrac{1}{2}(1+4\beta\alpha-\alpha^2) \pm \tfrac{1}{2}\sqrt{(1-\alpha)^2\left[(1+\alpha)^2-8\alpha\beta\right]}\,. \quad (A.7)$$

As a result of taking the square of (A.6), $\omega_{\pm}$ either solve eq. (A.6) or the equation $(1+\omega)^{1/2} = -(\omega+2\beta)/(\omega/\alpha+2\beta)$, and we must verify that the solutions (A.7) indeed satisfy (A.6).

The following results follow in a straightforward way from eqs. (A.6) and (A.7):

i) For $\alpha > (1-\beta)^{-1}$, ω_+ and ω_- both solve eq. (A.6) and are real. Since $\omega_+ > 0$, there is a mode of the form (A.2) that is unstable. One can show from eq. (3) and the definitions of α and β that

$$\frac{dV}{dT^b} \gtrless \frac{dV_{ss}}{dT_{ss}^b} \leftrightarrow \alpha \gtrless (1-\beta)^{-1}, \quad (A.8)$$

where the $>$ and $<$ sign correspond to points of type A and B respectively. Hence the above result implies that steady state solutions of type A are always *unstable*. The line $\alpha = (1-\beta)^{-1}$ separating type A and type B solutions is drawn in figs. 2 and 7 with a dashed line.

ii) For points of type B ($\alpha < (1-\beta)^{-1}$), both ω_+ and ω_- are solutions of eq. (A.6) with $\mathrm{Re}\,\omega_{\pm} > 0$ if $\beta < (\alpha-\alpha^{-1})/4$. At the line $\beta = (\alpha-\alpha^{-1})/4$, drawn in figs. 2 and 7 with a solid line, $\mathrm{Im}\,\omega_+$ varies continuously from 0 at the point $\alpha = 3$, $\beta = 2/3$ to $(1+\sqrt{5})^{3/2}/\sqrt{2} \approx 4.12$ if $\beta = 1$. In the limit $\Gamma \ll V_{ss}^2/4\kappa$, when $\beta \approx 1$, comparison of the above result with (A.2) shows that in this regime, the period of the oscillations is about

$$\frac{\pi}{4.12}\tau_m \approx 0.76\tau_m \approx \frac{6.1\kappa}{V_{ss}^2} \quad (A.9)$$

justifying our earlier contention that the period is of the order of τ_m.

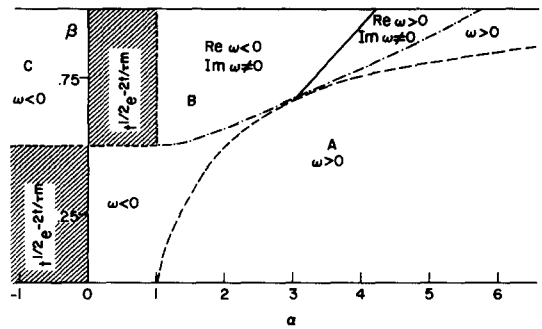

Fig. 7. The largest eigenvalue ω of the equations linearized around a steady state solution. At the solid line ($\beta = (\alpha - \alpha^{-1})/4$), $\mathrm{Re}\,\omega = 0$ while $\mathrm{Im}\,\omega \neq 0$. The chain-dotted line ($\beta = (\alpha+1)^2/8\alpha$) separates the points where ω is complex from those where ω is real, and the dashed line ($\alpha = (1-\beta)^{-1}$) separates the points of type A and B. For $0 < \alpha < 1$, $\beta > 1/2$ and $\alpha < 0$, $\beta < 1/2$, the perturbations decay asymptotically as (A.1), as indicated in the figure.

All point of type B to the left of the solid line are stable. However, for $\alpha < 1$, $\beta > 1/2$, $\omega_\pm$ do not solve eq. (A.6) and all perturbations decay as (A.1).

iii) For the points of type B with $\beta > (\alpha+1)^2/8\alpha$, $\mathrm{Im}\,\omega_\pm \neq 0$. The line $\beta = (\alpha+1)^2/8\alpha$ is drawn in fig. 7 with a dotted-dashed line. The conditions on the real part of $\omega_\pm$, which controls the stability, have been discussed in ii).

iv) Points of type C ($\alpha < 0$) are always stable. For $\beta > \frac{1}{2}$, only ω_- solves eq. (A.6) and perturbations decay asymptotically as in (A.2), while for $\beta < \frac{1}{2}$, the asymptotic decay is as in (A.1).

Appendix B

Derivation of the coefficients (10)

To derive the coefficients a_1, a_2 and a_3 in eq. (10), we expand (4) near the point $\alpha = 3$, $\beta = 2/3$. Using the variable $v \equiv V(t)/V_{ss} - 1$, we write $V(t-\tau) = V_{ss}(1 + v - \dot{v}\tau + \frac{1}{2}\ddot{v}\tau^2 + \cdots)$. Using τ as integration variable in (4) and neglecting the initial value term, we get with the aid of this expansion

$$\Delta T^{\mathrm{b}}(t) = \frac{q}{(4\pi\kappa\Gamma)^{1/2}} \int_0^\infty \mathrm{d}\tau\, \tau^{-1/2} \exp\left[-\tau - \frac{V_{ss}^2 \tau}{4\kappa\Gamma}\left(1 + v - \frac{1}{2}\tau\dot{v} + \frac{1}{6}\tau^2\ddot{v}\right)^2 \right]$$

$$\times V_{ss}(1 + v - \tau\dot{v} + \tfrac{1}{2}\tau^2\ddot{v} + \cdots) = \Delta T_{ss}^{\mathrm{b}} \int_0^\infty \mathrm{d}\tau\, \tau^{-1/2} \mathrm{e}^{-\tau(1+\gamma)} \Big\{ 1 + v(1 - 2\tau\gamma) + (\gamma\tau - 1)\dot{v}\tau$$

$$- \tau^2\ddot{v}\left(\frac{2\tau}{3} - 1/2\right) - v^2(6\tau - 8\tau^2) + 8\dot{v}v\tau - \frac{5}{2}\tau^3\dot{v}^2 + \cdots \Big\}. \quad \text{(B.1)}$$

Here $\gamma \equiv V_{ss}^2/4\kappa\Gamma = \beta/(1-\beta)$ and only terms of order v, $\dot{v}$, $\ddot{v}$, v^2, $\ddot{v}v$ and $\dot{v}^2$, have been retained. In the terms proportional to $\ddot{v}$, v^2, $\dot{v}v$, and $\dot{v}^2$, we take $\gamma = 2$, the values in the bifurcation point. After evaluation of the integrals we then arrive at

$$\Delta T^{\mathrm{b}}(t) = \Delta T_{ss}^{\mathrm{b}} \Big\{ 1 + (1-\beta)v + \frac{1}{4}\delta\beta\dot{v} - \frac{1}{6^3}\ddot{v} - \frac{1}{3}v^2 + \frac{2}{3}v\dot{v} - \left(\frac{5}{12}\right)^2 \dot{v}^2 \Big\}. \quad \text{(B.2)}$$

Expansion of $\Delta T^{b}(t)$ using the variable α and V'' (defined in eq. (11)) yields

$$\Delta T^{b}(t) = \Delta T^{b}_{ss}\left(1 + \alpha^{-1}v - \tfrac{1}{2}\alpha^{-3}V''v^2 + \cdots\right). \tag{B.3}$$

Combination of eqs. (B.2) and (B.3) finally yields

$$\ddot{v} - 54\delta\beta\dot{v} - 24(\delta\alpha - 9\delta\beta)v + 72\left(1 - \frac{1}{18}V''\right)v^2 - 144v\dot{v} + \frac{75}{2}\dot{v}^2 = 0. \tag{B.4}$$

From this follow the expressions for a_1, a_2 and a_3, given in eq. (10).

Notice that the coefficient of the term proportional to $\dot{v}$ does not agree with eq. (9). This is due to the fact that this factor gets renormalized by terms involving the third order derivative that have been left out in the above analysis. To see this, consider the equation $c\dddot{v} + \ddot{v} - \mu\dot{v} - \nu v = 0$, with c of order unity and μ and ν small. The characteristic polynomial then reads $c\omega^3 + \omega^2 - \mu\omega - \nu = 0$. Retaining only the dominant terms, we may write $c\omega^3 + \omega^2 - \mu\omega - \nu \approx (c\omega + 1)[\omega^2 - (\mu - \nu/c)\omega - \nu] = 0$. Thus, while in the neighborhood of the $\mu = \nu = 0$ critical point the system is well described by a second order equation, the coefficient of the $\dot{v}$ term gets renormalized by the coefficient of the $\ddot{v}$ term [46].

Appendix C

Description of the numerical solution

Our numerical analysis was based on solving eq. (4) with τ rather than x as the integration variable in the first integral. We used a fixed time step Δt; given the values of T^{b} and V at time $t, t - \Delta t, t - 2\Delta t, \ldots$, an initial guess for $V(t + \Delta t)$ was made. Using this estimate in the integrals in the right-hand side of eq. (5), $T^{b}(t + \Delta t)$ was calculated using (4) and the resulting $V(t + \Delta t)$ using eq. (2). If the updated value of $V(t + \Delta t)$ differed more than 10^{-5} from the previous value, we recalculated $T^{b}(t + \Delta t)$ using the updated values in the integral. The time integral in eq. (4) was cut off at $\tau = 1.4$ (the contribution from the rest of the integral is typically of the order of 10^{-8}), and the integral from $\tau = 0$ to $\tau = 1$ was done with equally spaced grid in the variable $\tau^{1/2}$ rather than τ. Integrals were calculated using Simpson's rule and the time step used in the calculation was $0.00032 \approx \tau_m/500$.

References

[1] For general reviews see e.g. R.F. Sekerka, in: Crystal Growth, an Introduction, P. Hartman, ed. (North-Holland, Amsterdam, 1973); J.S. Langer, Rev. Mod. Phys. 52 (1980) 1.

[2] R.F. Sekerka, Physica 12D (1984) 212 (these proceedings).

[3] G. Gore, Phil. Mag. 9 (1855) 73.

[4] C.C. Coffin and S. Johnston, Proc. Roy. Soc. A146 (1934) 564.

[5] W. Lotmar, Helv. Phys. Acta 18 (1945) 369.

[6] A. Götzberger, Z. Physik 142 (1955) 182.

[7] F.M. Aymerich and A. Delunas, Phys. Stat. Sol. A31 (1975) 165.

[8] C.E. Wickersham, G. Bajor and J.E. Greene, Solid State Commun. 27 (1978) 17; C.E. Wickersham, Ph.D. Thesis, University of Illinois at Urbana-Champaign (1978).

[9] T. Takamori, R. Messier and R. Roy, Appl. Phys. Lett. 20 (1972) 201; J. Mat. Sci. 9 (1974) 159.

[10] R. Messier, T. Takamori and R. Roy, Solid State Commun. 16 (1975) 311.

[11] A. Mineo, A. Matsuda, T. Kurosu and M. Kikuchi, Solid State Commun. 13 (1973) 329.

[12] A. Matsuda, A. Mineo, T. Kurosu and M. Kikuchi, Solid State Commun. 13 (1973) 1165.

[13] M. Kikuchi, A. Matsuda, T. Kurosu, A. Mineo and K.J. Callanan, Solid State Commun. 14 (1974) 713.
[14] K.J. Callanan, A. Matsuda, A. Mineo, T. Kurosu and M. Kikuchi, Solid State Commun. 15 (1974) 119.
[15] R.B. Gold, J.F. Gibbons, T.J. Magee, J. Peng, R. Ormond, V.R. Deline and C.A. Evans, in: Laser and Electron Beam Processing of Materials, C.W. White and P.S. Peercy, eds. (Academic Press, New York, 1980), p. 221.
[16] J.C.C. Fan, H.J. Zeiger, R.P. Gale and R.L. Chapman, Appl. Phys. Lett. 36 (1980) 158.
[17] R.L. Chapman, J.C.C. Fan, H.J. Zeiger and R.P. Gale, Appl. Phys. Lett. 37 (1980) 292.
[18] H.J. Zeiger, J.C.C. Fan, B.J. Palm, R.P. Gale and R.L. Chapman, in: Laser and Electron Beam Processing of Materials, C.W. White and P.S. Peercy, eds. (Academic Press, New York, 1980), p. 234.
[19] R.L. Chapman, J.C.C. Fan, H.J. Zeiger and R.P. Gale, in: Laser and Electron-Beam Solid Interactions, J.F. Gibbons, L.D. Hess and T.W. Sigmon, eds. (North-Holland, Amsterdam, 1981), p. 81.
[20] H.J. Zeiger, J.C.C. Fan, B.J. Palm, R.L. Chapman and R.P. Gale, Phys. Rev. B25 (1982) 4002.
[21] C.E. Wickersham, Solid State Commun. 34 (1980) 907.
[22] H.J. Leamy, W.L. Brown, G.K. Celler, G. Foti, G.H. Gilmer and J.C.C. Fan, Appl. Phys. Lett. 38 (1981) 137; ref. 19, p. 89.
[23] R. Koba and C.E. Wickersham, Appl. Phys. Lett. 40 (1982) 672.
[24] O. Bostanjoglo, Phys. Stat. Sol. A70 (1982) 473.
[25] L.N. Aleksandrov and F.L. Edelman, Surf. Sci. 86 (1979) 222.
[26] G. Auvert, D. Bensahel, A. Georges, V.T. Nguyen, P. Henoc, F. Morin and P. Coissard, Appl. Phys. Lett. 38 (1981) 613.
[27] G. Auvert, D. Bensahel, A. Perio, V.T. Nguyen and G.A. Rozgonyi, Appl. Phys. Lett. 39 (1981) 724.
[28] R.A. Lemons and M.A. Bösch, Appl. Phys. Lett. 39 (1981) 343.
[29] S.V. Krishnaswamy, R. Messier, P. Swab, L.L. Tongson and K. Vedam, J. Electr. Mat. 10 (1981) 433.
[30] V.M. Kuz'menko and V.I. Mel'nikov, Sov. Phys. JETP 55 (1982) 474.
[31] Zeiger and coworkers (ref. 20) have analyzed this case in some detail. However, they make the physically questionable approximation that the temperature at the boundary remains constant despite possible variations in the interface velocity. This approximation is inconsistent with the mechanism leading to propagating oscillatory crystallization waves discussed here. Furthermore, as noted by the authors, it also causes numerical convergence problems and predicts unphysical negative interface velocities at low substrate temperatures.
[32] G.H. Gilmer and H.J. Leamy, ref. 15, p. 227.
[33] Measurements by Koba and Wickersham (ref. 23) suggest that L is rather the latent heat per unit volume less a correction term (probably due to heat radiation) inversely proportional to the height of the layer.
[34] See e.g. R.F. Sekerka, in: "Proc. Int. School of Crystallography," Erice, 1981, (Reidel, Dordrecht, 1982).
[35] See e.g., H.S. Carslaw and J.C. Jaeger, Conduction of Heat in Solids, (Oxford Univ. Press, London, 1959); P.M. Morse and H. Feshbach, Methods of Theoretical Physics (McGraw-Hill, New York, 1953).
[36] J. Guckenheimer, IEEE Trans. Circuits Syst. 27 (1980) 982.
[37] J. Guckenheimer, in: New Approaches to Nonlinear Problems in Dynamics, P.J. Holmes, ed. (SIAM, Philadelphia, 1980); "Multiple Bifurcation Problems of Codimension 2", preprint.
[38] M. Shaerer, SIAM J. Math. Anal. 11 (1980) 365.
[39] H.R. Brand, P.C. Hohenberg and V. Steinberg, Phys. Rev. A27 (1983) 591.
[40] P.H. Coullet and E.A. Spiegel, "Amplitude Equations for Systems with Competing Instabilities", preprint.
[41] A. Andronov, E. Leontovich, I. Gordon and A. Maier, The Theory of Bifurcations of Plane Dynamical Systems (Wiley, New York, 1973).
[42] For experimental evidence for these effects see Wickersham's thesis, ref. 8, p. 269.
[43] W.W. Mullins and R.F. Sekerka, J. Appl. Phys. 34 (1963) 323; 35 (1964) 444.
[44] D.J. Wollkind, in: Preparation and Properties of Solid State Materials, vol. 4, W.R. Wilcox, ed. (Marcel Dekker, New York, 1979).
[45] M.J. Feigenbaum, J. Stat. Phys. 19 (1978) 25; 21 (1979) 669.
[46] Therefore, α in eq. (5) of ref. 39 should be replaced by $\alpha + \beta\gamma$.